

Pinched optical-vortex soliton

Anton M. Deykoon and Grover A. Swartzlander, Jr.

Department of Physics, Worcester Polytechnic Institute, Worcester, Massachusetts 01609-2280

Received April 4, 2000; revised manuscript received January 2, 2001

The fast contraction, or pinching, of optical vortices in both thermal and Kerr self-defocusing media is investigated by numerical techniques. For the thermal case, heat diffusion across the vortex core is described, and the heretofore unexplained stability of optical-vortex solitons in thermal media is explained. © 2001 Optical Society of America

OCIS codes: 190.4420, 190.5940, 190.3270, 160.4330.

1. INTRODUCTION

Optical vortices appear as doughnut modes of a cylindrical waveguide,^{1,2} as Laguerre-Gaussian modes of a laser cavity,³⁻⁵ and as spontaneous features in large-aperture lasers.^{6,7} They may be produced by computer-generated holograms,⁸⁻¹⁰ mode converters,¹¹ or scattering objects.¹² In a self-defocusing medium, vortices may propagate as optical-vortex solitons¹³ (OVS's), owing to a balance between diffraction and nonlinear refraction.¹⁴ The size of the OVS, w_{OVS} , decreases as the nonlinear refractive-index difference between the dark vortex core and the bright background, $|\Delta n|$, increases. Experimentally we found earlier that if the initial vortex size, $w_{v,0}$, is larger than the soliton size, the vortex core may abruptly contract, and a high-intensity shock wave could radiate symmetrically from the vortex core.¹⁵ This pinching of the vortex core may be an advantageous feature for applications of nonlinear guided-wave phenomena, such as optical modulators or transistors, where the vortex beam induces a dynamic waveguide for a signal-carrying beam. Like a field-effect transistor, the strength of the guided signal will vary with the degree of pinching. Here we give the first detailed report, to our knowledge, of the characteristics of the collapsing vortex in both Kerr and nonlocal fluence-dependent nonlinear mechanisms. This comparison is necessary because nonlinear refractive media are not strictly Kerr-like, but rather exhibit some degree of nonlocality (or diffusion), such as heat-absorbing liquids,¹⁶⁻¹⁹ alkali vapors,²⁰⁻²³ or electrically biased photorefractive crystals.²⁴ We examine a thermal liquid having the same thermo-optical properties as those in our earlier experiments with methanol.¹⁵ The shock front surrounding the OVS, which may be sustained over many characteristic nonlinear lengths, is also of physical interest; however, it is not the main subject of this study.

An optical vortex is characterized by a harmonic transverse phase profile around its center and an intensity profile that vanishes at the center. The initial electric field E of a vortex placed in the center of a planar Gaussian beam of size w_g and peak intensity $I_0 = E_0^2$ may be written as

$$E(\rho, \theta) = E_0 \tanh(\rho/w_{v,0}) \exp(-\rho^2/w_g^2) \exp(i\theta), \quad (1)$$

where $w_{v,0}$ is the characteristic vortex size and (ρ, θ) are circular coordinates in the beam cross section. Here we model the nonlinear propagation of a vortex beam, of wavelength $\lambda = 0.514 \mu\text{m}$ and sizes $w_g = 5.0 \text{ mm}$ and $w_{v,0} = 0.4 \text{ mm}$, through a medium of length $L = 200 \text{ mm}$. The material is thin, since the length is less than the characteristic longitudinal diffraction length of both the vortex core ($kw_{v,0}^2/2 \approx 1 \text{ m}$) and the Rayleigh range ($kw_g^2/2 \approx 350 \text{ m}$) for the Gaussian beam, where $k = 2\pi n_0/\lambda$ is a wave number in the medium. We note, however, that the characteristic nonlinear length scale, $1/k\Delta n$, may be less than the cell length in some cases.

The vortex propagation dynamics of this initial beam is found by solving the nonlinear Schrödinger equation:

$$-2ik(\partial E/\partial z) + \nabla_{\perp}^2 E + 2k^2 \Delta n E/n_0 = 0, \quad (2)$$

where $\nabla_{\perp}^2 = \partial^2/\partial x^2 + \partial^2/\partial y^2$ and where Δn varies with intensity or fluence and couples to the heat equation in a thermal medium. For a given initial vortex size the propagation dynamics of the beam depends on the background intensity or fluence and may result in diffraction of the core, contraction of the core, or soliton propagation.

Case 1. Kerr Material

In Kerr media, $\Delta n = n_2|E|^2$, where $n_2 < 0$ is the nonlinear defocusing coefficient of the refractive index and $|E|^2$ is the local intensity of the beam. When the initial vortex-core size matches the soliton size, $w_{v,0} = w_{\text{OVS}}$, where

$$w_{\text{OVS}} \approx 1.27/k \sqrt{|\Delta n|/n_0}, \quad (3)$$

the vortex soliton core sheds little radiation as it propagates throughout the medium, assuming $w_{v,0} \ll w_g$ in Eq. (1). This is equivalent to the condition that the background intensity in Eq. (1) equals the soliton intensity,¹³ $I_0 = I_{\text{sol}}$, where $I_{\text{sol}} = (1.27/w_{v,0}k)^2 n_0/|n_2|$. The power of a Gaussian beam with a small vortex¹⁰ ($w_{v,0} \ll w_g$) is roughly $P = I_0 \pi w_g^2/2$, and thus the power required for soliton propagation is $P_{\text{cr}} \approx (0.806 \pi n_0/|n_2|k^2)(w_g/w_{v,0})^2$. It is well known that a 1 + 1-dimensional beam having an arbitrary size may be decomposed into soliton and radiation components.^{25,26} Similarly, we find that when the initial vortex core is larger than the soliton size, $w_{v,0} > w_{\text{OVS}}$, or, equivalently,

when $P > P_{cr}$ (or $I_0 > I_{sol}$), the propagating vortex contracts in size and radiates a bright diffraction ring. Light is refracted toward the core, and thus much of this radiation initially implodes.

The intensity profiles near the vortex core at different propagation distances are presented in Fig. 1 for the case $P/P_{cr} = 140$ ($\Delta n = 7 \times 10^{-6}$). We find the initially large vortex core [see Fig. 1(a)] collapses by a factor of 12 after propagating a distance $z = 152$ mm, as shown in Fig. 1(b). Further propagation results in a high-intensity ring around the vortex, as shown in Fig. 1(c) for $z = 200$ mm. Note that intensity of the imploded wave in Fig. 1(c) is higher than the background intensity $I_{bg}^{(c)}$. The persistence of this ring over long distances suggests that it represents a nonlinear guided mode at the perimeter of the high-index vortex core.

Our main concern in this paper is the contracting core size in the propagating beam. Assuming a core profile that varies as $\tanh(\rho/w_v)$, we measure the background intensity I_{bg} outside the bright ring (see Fig. 1) and determine the radius of the core, w_v , at the value $I = I_{bg} \tanh^2(1)$. The core size as a function of propagation distance is plotted in Fig. 2 for the same conditions used in Fig. 1. The propagation dynamics has three distinct phases: first a slow contraction of the vortex core, then a rapid collapse near $z = Z_c$, and finally a relaxation for $z \gg Z_c$. A numerically determined value of the characteristic collapse distance, Z_c , is found where the slope dw_v/dz has an extremum, as shown in Fig. 2. An analytical estimation of this pinching distance, Z_{pinch} , may be determined by comparing the fundamental nonlinear scaling distances²⁷ with the distances in our problem; e.g., we set $X_{NL}/Z_{NL} = w_{v,0}/Z_{pinch}$, where $X_{NL} = k^{-1}(\Delta n_0)^{-1/2}$, $Z_{NL} = (k\Delta n_0)^{-1}$, and $\Delta n_0 = 2P/(\pi w_g^2)$

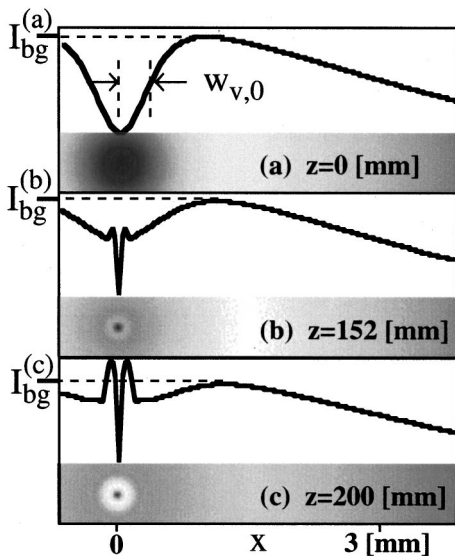


Fig. 1. Formation of an overshooting ring around the vortex core. (a) The intensity profile at the input is transformed into an OVS with a bright ring around it at (b) $z = 152$ mm and (c) $z = 200$ mm. Parameters of the beam are $w_g = 5$ mm, $w_{v,0} = 0.4$ mm, $P = 1.4$ W, and wavelength $\lambda = 0.514$ μ m. Nonlinear coefficient $n_2 = -2 \times 10^{-6}$ cm²/W, refractive-index change $\Delta n = 7 \times 10^{-6}$, the corresponding size of the OVS is $w_{ovs} = 34$ μ m, and $Z_{pinch} = 150$ mm.

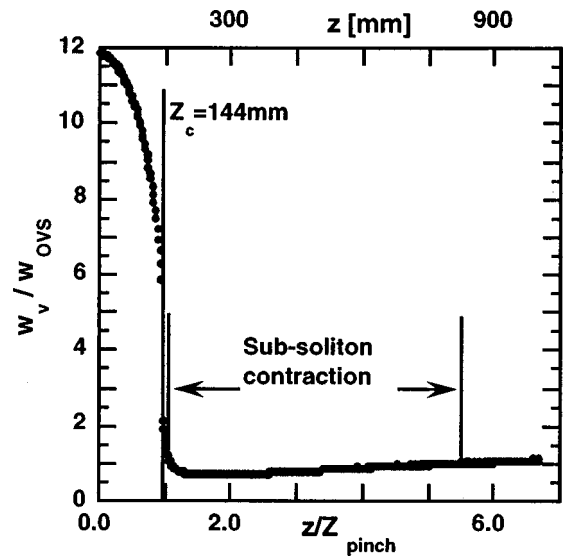


Fig. 2. Initially large vortex core contracts to a subsoliton size of $w_v^{min} = 23$ μ m in a Kerr material (parameters are identical to those in Fig. 1). The vortex remains contracted to subsoliton size over ~ 60 characteristic nonlinear distances. As expected, the collapse distance, Z_c , is found to agree with the theoretical value of Z_{pinch} .

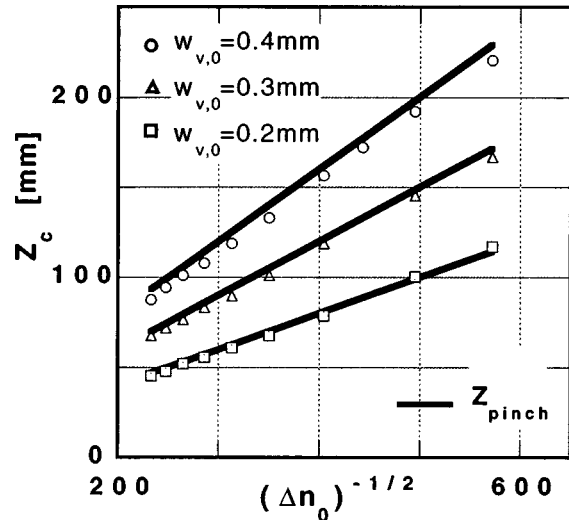


Fig. 3. Pinch distance Z_c as a function of the input refractive-index change $\Delta n_0 = n_2 P / (\pi w_g^2 / 2)$ in a Kerr nonlinear medium. Symbols represent numerically determined values of Z_c ; solid lines represent $Z_{pinch} = w_{v,0} / \sqrt{\Delta n_0}$.

is the characteristic refractive-index change at the input. Thus we find

$$Z_{pinch} = w_{v,0} / \sqrt{\Delta n_0}, \tag{4}$$

which agrees remarkably well with the numerically determined value of Z_c ($Z_c = 144$ mm and $Z_{pinch} = 150$ mm). Indeed, many simulations with different initial core sizes and intensities verify that $Z_c \approx Z_{pinch}$. In Fig. 3 we compare the numerically determined collapse distances Z_c (marked by symbols) with Eq. (4) (thick lines) for different values of Δn_0 and three different cases of an initially large vortex size. The agreement is good in all three cases.

After pinching, the vortex may surprisingly contract below the soliton size for prolonged propagation distances. For example, in Fig. 2 the core reaches 68% of the soliton size [Eq. (3)] at $z \approx 1.8Z_{\text{pinch}}$ and relaxes to w_{ovs} at $z/Z_{\text{pinch}} = 5.5$. Over this subsoliton contraction range we found that the bright shock ring described in Fig. 1 develops into a flat plateau (or shock region) that shrouds the OVS. This ring enhances the local intensity of the soliton and accounts for the contracted core size over a range that exceeds the characteristic nonlinear length, $Z_{\text{NL}} = 12$ mm, by a factor of 60.

Case 2. Thin Thermal Medium

Dark soliton phenomena may be readily investigated in thermal and other nonlinear media; however, the nonlocal effects of diffusion should be considered. In absorbing media such as slightly absorbing methanol, an optical vortex acts as an annular heat source and induces an inhomogeneous temperature distribution, T , that scales with the nonlinear index profile:

$$\Delta n(x, y, z, t) = (\partial n / \partial T) T(x, y, z, t), \quad (5)$$

where $\partial n / \partial T$ is a material parameter²⁸ and $T(x, y, z, t)$ is the temperature increase above the ambient value. We assume that the electronic nonlinearity and other mechanisms such as buoyancy, convection, and sound are negligible. Most liquids are self-defocusing with $\partial n / \partial T < 0$. The refractive index (or equivalently, the temperature) may be obtained by solving the heat equation:

$$\partial T(x, y, z, t) / \partial t = D \nabla_{\perp}^2 T + \alpha |E(x, y, z)|^2 / (c_p \rho), \quad (6)$$

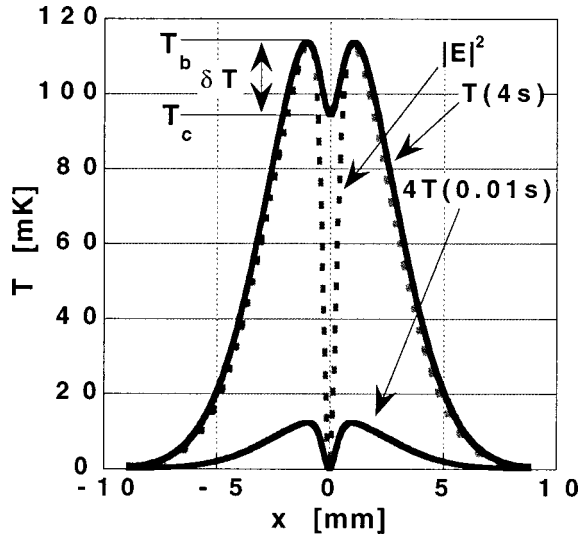


Fig. 4. Temperature profiles in a thin layer of absorbing liquid heated by an annular beam (dashed) with parameters listed in Table 1 at $t = 0.01$ s and 4 s. The temperature difference across the core, $\delta T = T_b - T_c$, varies with time.

where $D = \kappa / c_p \rho$ is a temperature-diffusion coefficient, κ is the heat-diffusion coefficient, $|E|^2$ is the optical intensity, α is the optical-absorption coefficient, c_p is heat capacity, and ρ is the density of the liquid. Compared with the transverse diffusion of heat, longitudinal diffusion is negligible, and thus we ignore $\partial^2 / \partial z^2$ in Eq. (6). In this subsection we assume a thin medium with a thickness $L \ll Z_c, Z_{\text{NL}}$, and we address a thick medium²⁹ below.

The light-induced temperature profile for a thin absorbing medium is shown in Fig. 4, assuming an annular heat source from an optical vortex and the parameters shown in Table 1. Owing to the dark core of the illuminating beam, the temperature distribution is cooler in the center of the beam than in the high-intensity regions, and therefore the refractive index is higher in the vortex core than it is along the bright rim. Consequently the vortex induces an effective cylindrical waveguiding structure, where the index difference between the core and the cladding is given by $\Delta n_g = (\partial n / \partial T)(T_c - T_b) = -(\partial n / \partial T) \delta T > 0$, where $T_c(T_b)$ is the temperature at the center of the core (along the rim) of the vortex, and $\delta T = T_b - T_c$, as demarked in Fig. 4.

The characteristic time for heat diffusion across the core is given by $t_v = w_{v,0}^2 / 8D = 0.2$ s. Thus for $t \ll t_v$ the temperature (see dashed curve in Fig. 4) is indistinguishable from the intensity profile, and thus the nonlinear optical effects of thermal and Kerr mechanisms are indistinguishable, as expected.¹⁶ In contrast, the effects of diffusion are clearly evident in the core region for $t \gg t_v$, as shown in Fig. 4. In both time regimes an inverted temperature profile exists in the core, which is favorable for an OVS.

The temperature inversion δT grows with time as long as the rate of background heating by absorption is larger than the rate of core heating by diffusion. The time evolution of $\delta T(t)$ is shown in Fig. 5 for two different values of $w_{v,0}$ (0.4 mm and 0.2 mm). When the rates of core and background heating are equal, δT reaches its maximum value; numerically we find that this occurs at a characteristic time

$$t_{\text{opt}} \approx w_{v,0} w_g / 7D, \quad (7)$$

assuming $w_{v,0} \ll w_g$. Thus the characteristic time for the buildup of the waveguide (Δn_g) is roughly $t_{\text{opt}} \approx (w_g / w_{v,0}) t_v$. For $t \ll t_{\text{opt}}$ the initial rate of growth of Δn_g is found by neglecting heat diffusion in Eq. (6): $\partial(\Delta n_g) / \partial t = (\partial n / \partial T) \alpha I_0 / (c_p \rho)$. Numerical modeling shows that the maximum value of Δn_g is proportional to t_{opt} : $\Delta n_{g,\text{max}} \approx (0.8)(\partial n / \partial T)(\alpha I_0 / c_p \rho) t_{\text{opt}}$. For the case $w_v = 0.4$ mm in Fig. 5, $t_{\text{opt}} = 3.2$ s, $\delta T = 19.5$ mK, $\Delta n_g = 7.6 \times 10^{-6}$, and the corresponding soliton size $w_{\text{ovs}} = 33$ μm .

At the other extreme where $t \gg t_{\text{opt}}$, heat diffusion dominates the dynamics of $\delta T(t)$. Diffusion is responsible for a logarithmically slow growth of the background

Table 1. Parameters of the Heat Source and Material Used to Produce Fig. 4

$w_{v,0}$ (mm)	w_g (mm)	I_0 (W/cm ²)	c_p (J/kg-K)	ρ (kg/m ³)	D (s/m ²)	$\partial n / \partial T$ (K ⁻¹)	α (m ⁻¹)
0.4	5	2.6	2500	790	10^{-7}	3.9×10^{-4}	3.6

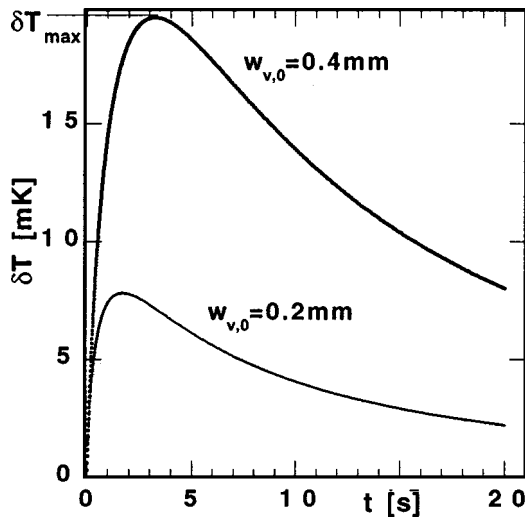


Fig. 5. Time evolution of the temperature difference δT for two input vortex sizes. The maximum of δT occurs at $t_{\text{opt}} = 3.2$ s when $w_{v,0} = 0.4$ mm, and $t_{\text{opt}} = 1.7$ s when $w_{v,0} = 0.2$ mm. Beam and material parameters are listed in Table 1.

temperature: $T_b = \alpha P \ln(1 + t/t_g)/(4\pi\kappa)$, where $t_g = w_g^2/8D$ is the characteristic time of the heat conduction across the entire beam.¹⁶ It also accounts for the slow heating of the vortex core and the gradual decrease of Δn_g , owing to the diffusion of heat from the bright rim of the vortex. The required index change, $\Delta n_g = 5.1 \times 10^{-8}$, for a vortex soliton of size $w_{\text{sol}} = w_{v,0} = 0.4$ mm can be sustained for a long time (320 s or more than $100t_{\text{opt}}$ in our system). Over such long time periods, convective flows develop within the thermal liquid, bringing cooler liquid into the beam. To account for the steady-state value of the OVS core size in experiments,¹⁵ we believe that the slow heating of the core is offset by the convected cooler liquid.

Case 3. Thick Thermal Medium

Let us now consider the propagation of a vortex beam through a thick thermal medium. As in the Kerr case, we assume a nonlinear cell of length $L = 200$ mm, in addition to the parameters listed in Table 1. Based on the foregoing thermal analysis in a thin layer, we expect the time variation of the induced waveguide (e.g., the temperature δT and refractive-index change Δn_g) to be similar to the results shown in Fig. 5. Consequently the pinching distance is expected to vary with time as $Z_{\text{pinch}}(t) \approx w_{v,0}/\sqrt{\Delta n_0(t)}$, where $\Delta n_0(t)$ is the time-varying refractive-index change at the input face. Thus on short ($t \ll t_{\text{opt}}$) or long ($t \gg t_{\text{opt}}$) time scales, the contraction may not be observed owing to small values of Δn_0 . The vortex is expected to collapse within the medium when $Z_{\text{pinch}}(t) < L$.

The vortex size, which is proportional to $1/\sqrt{\Delta n_0(t)}$ [see Eq. (3)], is also expected to vary with time. The numerically determined contraction of the vortex at the output face of the cell is shown in Fig. 6 over an 8-s exposure time at intensity $I_0 = 2.6 \text{ W/cm}^2$. This example confirms that $w_{v,0}$ contracts with time, goes through a minimum

(at $t = 3.1$ s), and then slowly expands. The collapse time is in a good agreement with the value expected from Fig. 5, namely, $t_{\text{opt}} = 3.2$ s.

As in the Kerr case, a bright ring may be expected to develop around the contracting vortex core. Indeed, the ring has been experimentally observed.¹⁵ Our numerical solutions of the coupled heat and nonlinear Schrödinger equations shown in Fig. 7 demonstrate the buildup of a bright ring at the output face of the medium for exposures up to 8 s at an incident intensity $I_0 = 2.6 \text{ W/cm}^2$. Before the ring appears, the vortex uniformly contracts by a factor of 2.2 within 0.40 s [see Figs. 7(a) and 7(b)]. With further contraction a bright ring develops around the perimeter of the vortex core [see Fig. 7(c)], reaching the maximum intensity of $I/I_0 = 0.58$ at $t = 2.7$ s. Then the

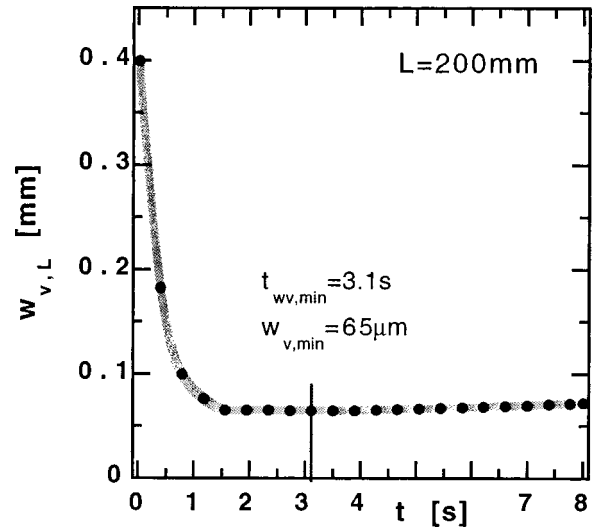


Fig. 6. Vortex size $w_{v,L}$ at the output face contracts to a minimum size $w_{v,\text{min}} = 65 \mu\text{m}$ at time $t_{wv,\text{min}} = 3.1$ s. Beam and material parameters are listed in Table 1. The gray curve is drawn to aid the eye.

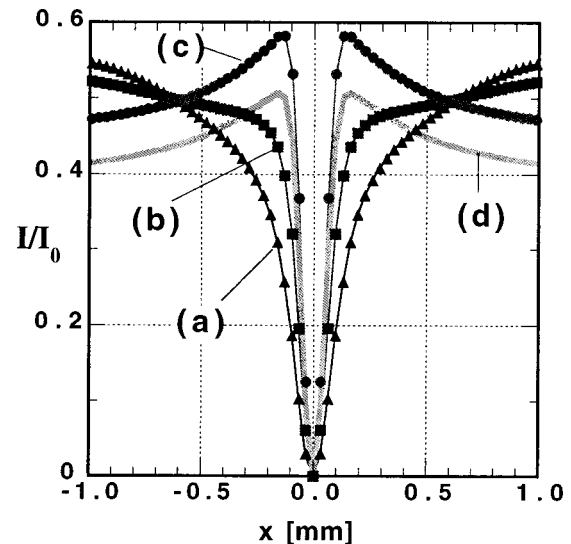


Fig. 7. Intensity profiles at the output face of a thermal medium of length $L = 200$ mm at time (a) $t = 0.002$ s, (b) $t = 0.40$ s, (c) $t = 3.1$ s, and (d) $t = 8.0$ s. Beam and material parameters are listed in Table 1.

vortex-core size reaches a minimum at $t = 3.1$ s. After this time the core slowly broadens, and the intensity of the ring diminishes owing to thermal diffusion [see Fig. 7(d)]. At much longer exposure times the ring may vanish, as was experimentally observed.¹⁵ Note that the normalized intensity in Fig. 7 is less than unity owing primarily to absorption.

2. COMPARISON BETWEEN KERR AND THERMAL NONLINEAR VORTICES

Let us now make a detailed comparison of the vortex contraction between thermal and Kerr media. To be relevant to experiments, we examine how an increase in the beam power affects the core size in these two media. The nonlinear refractive index varies with time in the thermal case, so we must select an appropriate exposure time for this comparison. For $t \ll t_{\text{opt}}$ the temperature (and refractive index) increases monotonically with intensity, and thus the thermal medium is similar to a Kerr medium having a time-dependent (or fluence-dependent) nonlinear coefficient, $n_2(t)$. We found that choosing $t_0 = 1.5 \text{ s} \approx 0.5t_{\text{opt}}$ is sufficient to demonstrate the difference between thermal and Kerr media. Let us compare a Kerr medium having $n_2 = -2 \times 10^{-6} \text{ cm}^2/\text{W}$ with a thermal medium (see Table 1) having $n_{2,\text{eff}} = (\partial n/\partial T) \times \delta T(1.5 \text{ s})/I_0 = -2.6 \times 10^{-6} \text{ cm}^2/\text{W}$, where $\delta T = 17 \text{ mK}$ and $I_0 = 2.6 \text{ W/cm}^2$. The beam parameters and propagation distance, $L = 200 \text{ mm}$, are the same for both media.

At this intensity the theoretical vortex soliton size [Eq. (3)] is expected to reach $w_{\text{ovs}} = 40 \mu\text{m}$ in the Kerr material, and generally varies as $1/P^{1/2}$ as shown in Fig. 8 (solid curve). As expected, our numerical results show that a large initial core ($400 \mu\text{m}$) indeed contracts with increasing power for both media (see gray curves in Fig. 8). Furthermore, in both cases the core size tends to converge toward the theoretical value at high power ($>1 \text{ W}$). At low powers the vortex did not contract to the size of a soliton because the pinching distance was larger than the cell length ($L < Z_{\text{pinch}}$ for $P < 0.75 \text{ W}$).

For the Kerr medium the power dependence of the output vortex size in Fig. 8 may be interpreted with Fig. 2. The abscissas of both figures are related: $z/Z_{\text{pinch}} \propto P^{1/2}$, and thus Fig. 2 may be mapped into Fig. 8. Thus we assert that the power-dependent vortex size shown in Fig. 8 exhibits a gradual contraction as the power increases from zero, followed by pinching at $P \geq 0.75 \text{ W}$ and then subsoliton contraction at $P = 2 \text{ W}$. The minimum estimated pinching power for a cell of length $L = 200 \text{ mm}$ may be calculated by setting $Z_{\text{pinch}} = L$ in Eq. (4): $P_{\text{pinch}} = (w_{v,0}/L)^2(\pi w_g^2/2|n_2|) = 0.78 \text{ W}$, which is in good agreement with the numerically determined value of 0.75 W .

Next we describe the thermal results shown in Fig. 8. Recalling that $n_{2,\text{eff}} = -2.6 \times 10^{-6} \text{ cm}^2/\text{W}$ has a larger magnitude than the Kerr coefficient does, the vortex-contraction effect is expected to be more pronounced in the thermal medium. Indeed, for power $P < 0.8 \text{ W}$ we find that the core size rapidly decreases with power, and unlike the Kerr case, the descent is almost linear, with no sudden collapse. For $P > 0.8 \text{ W}$ the contraction exhibits

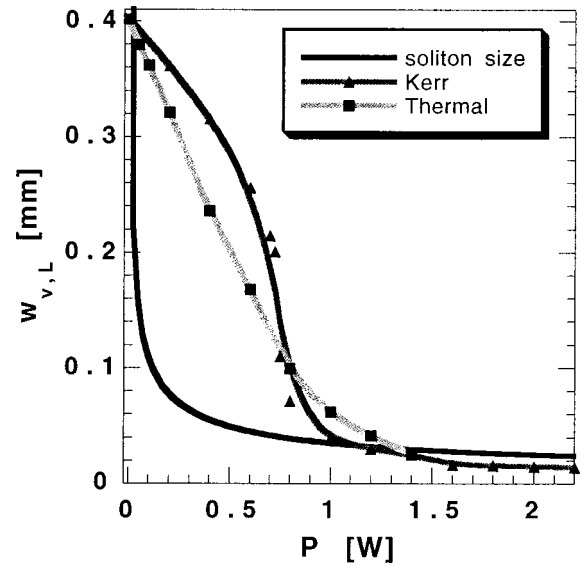


Fig. 8. Output vortex size as a function of incident power. Triangles represent the Kerr medium ($n_2 = 2 \times 10^{-6} \text{ cm}^2/\text{W}$), and squares represent the thermal medium ($\alpha = 3.6 \text{ m}^{-1}$, $t = 1.5 \text{ s}$). The OVS size $w_v = 1.27/k \sqrt{\Delta n/n_0}$ is shown for comparison by a solid curve. Gray curves are drawn to aid the eye.

a saturation owing to thermal diffusion across the contracted vortex core. That is, the temperature and index changes across the core saturate. Indeed, Fig. 5 shows that δT is reduced by approximately one half when the core size is halved. This saturation effect prevents the core from collapsing rapidly.

In comparison we see regimes where either the Kerr or the thermal media have smaller core sizes. At $P \approx 1.5 \text{ W}$, both mechanisms converge to roughly the same value as the Kerr soliton size. An estimate of the output vortex size may be found from Eq. (3). Let us estimate the core size at $P = 1.2 \text{ W}$ and $t = 1.5 \text{ s}$. Since the temperature change scales with power as $\delta T(P_2) = (P_2/P_1)\delta T(P_1)$, we may use Fig. 5 as a calibration graph: $\delta T(1.0 \text{ W}, 1.5 \text{ s}) = 17 \text{ mK}$, and thus $\delta T(1.2 \text{ W}, 1.5 \text{ s}) = 20 \text{ mK}$. The corresponding refractive-index change is $\Delta n_0 = -8.0 \times 10^{-6}$. From Eq. (3) we calculate the soliton size to be $w_{\text{ovs}} = 32 \mu\text{m}$. In comparison, our numerical solution, shown in Fig. 8, predicts $w_v = 41 \mu\text{m}$, which is 22% greater than our estimate.

Summarizing the discussion of Fig. 8, we find that in order to observe a contracted vortex having the size of an OVS at the output, the incident power must exceed $P_{\text{pinch}} = (w_{v,0}/L)^2(\pi w_g^2/2|n_2|)$ in the Kerr medium. In the thermal medium the nonlinear coefficient n_2 has to be found numerically for a specific vortex size and time. The diffusion of heat across the vortex core saturates the refractive-index change, which therefore limits the contraction of the core.

3. SUMMARY

The core of an optical vortex may propagate as a soliton or even pinch to a subsoliton size in a self-defocusing medium if the nonlinear refractive-index change across the vortex core is sufficient to overcome spreading owing to diffraction. Although a large index change may be

achieved in thermal media, the diffusion of heat introduces spatio-temporal complications. To discern between Kerr and thermal effects we numerically determined the propagation characteristics of an optical vortex. In both media the vortex core contracts and a bright ring is generated around the vortex core when the initial core size is larger than the soliton size. After the contraction, the vortex size increases adiabatically, owing to both the gradual radiation of the bright ring, which exists over many characteristic nonlinear distances, and the blooming of the entire beam. The propagation distance characterizing this contraction phenomenon is defined as the pinching distance, which is inversely related to the square root of the beam power. In the Kerr case the vortex core collapses to the soliton (or subsoliton) size after propagation over the pinching distance. In the thermal medium, nonlinear refraction varies with time, and thus the pinching distance and the output vortex size are time dependent. Solving the heat equation numerically, we find an expression for the optimal time at which the refractive-index change across the vortex core reaches the maximum value.

For a long exposure time, heat diffusion into the core causes a slow increase of the core size. We found, however, that the negative temperature difference between the core and the rim of a vortex exists over a long time interval (a minute and more) so that the vortex is expected to remain contracted over a prolonged period of time. The convection of cool liquid into the heated core can offset this heating, thereby allowing a steady-state core size.

APPENDIX A

Our numerical code solves the $(2 + 1)$ D nonlinear Schrödinger equation [Eq. (2)] coupled to the $(3 + 1)$ D heat equation [Eq. (6)]. The coupling occurs through the temperature change in the medium, which is stored in a three-dimensional array $T = T(x, y, m\Delta z)_{t=n\Delta t}$, where n is the number of time steps elapsed after turning on the laser, and m is an index corresponding to the spatial increments along the direction of propagation, z . The initial temperature distribution is uniform, $T(x, y, m\Delta z)_{t=0} = 0$. Let us review a single step in time, $n\Delta t \leq t < (n + 1)\Delta t$. The input electric field $E(x, y, 0)$ is generated according to Eq. (1) and propagated through the self-defocusing medium in the z direction by solving Eq. (2) with the split-step method.³⁰ The refractive-index change for the nonlinear portion of step m is calculated as $(\partial n/\partial T)T(x, y, m\Delta z)_{t=n\Delta t}$. As the beam propagates in space, the temperature distribution at each transverse plane $z = m\Delta z$ is updated for the next time step, $(n + 1)\Delta t$, according to the finite-difference scheme,

$$\begin{aligned} T(x, y, z)_{t=(n+1)\Delta t} &= T(x, y, z)_{t=n\Delta t} + \Delta t(D\nabla_{\perp}^2 T(x, y, z)_{t=n\Delta t} \\ &\quad + \alpha|E(x, y, z)_{t=n\Delta t}|^2/c_p\rho), \end{aligned}$$

where ∇_{\perp}^2 is Laplacian in the transverse plane (x, y) . The transverse Laplacian in both the nonlinear Schrö-

ding equation and the heat equation was calculated with the aid of the fast Fourier transform, which automatically assumes reflecting boundary conditions. The numerical grid was made sufficiently large compared with the beam size to avoid aliasing. High stability of the finite-difference scheme for the heat equation in the Fourier domain allowed for a large value of Δt .

ACKNOWLEDGMENTS

This research was supported by a grant from the Research Corporation (Cottrell Scholars Award) and the National Science Foundation (Young Investigator Award). We thank C. T. Law (University of Wisconsin, Milwaukee, Wisconsin) and A. A. Zozulya (Worcester Polytechnic Institute, Worcester, Massachusetts) for insightful discussions on numerical techniques. G. Swartzlander may be contacted at the Optical Sciences Center, University of Arizona, Tucson, Arizona 85721.

REFERENCES

1. G. Goubau and F. Scherwing, "On the propagation of electromagnetic wave beams," *IRE Trans. Antennas Propag.* **9**, 248–256 (1961).
2. R. E. Collin, *Field Theory of Guided Waves*, 2nd ed. (IEEE, New York, 1991), Chap. 5.
3. J. M. Vaughan and D. V. Willetts, "Temporal and interference fringe analysis of TEM₀₁* laser modes," *J. Opt. Soc. Am.* **73**, 1018–1021 (1983).
4. A. E. Siegman, *Lasers* (University Science, Mill Valley, Calif., 1986).
5. F. B. de Colstoun, G. Khitrova, A. V. Fedorov, T. R. Nelson, C. Lowry, T. M. Brennan, B. G. Hammons, and P. D. Maker, "Transverse modes, vortices and vertical-cavity surface-emitting lasers," *Chaos, Solitons Fractals* **4**, 1575–1596 (1994).
6. P. Couillet, L. Gil, and F. Rocca, "Optical vortices," *Opt. Commun.* **73**, 403–408 (1989).
7. M. Brambilla, M. Cattaneo, L. A. Lugiato, R. Pirovano, F. Pratti, A. J. Kent, G. L. Oppo, A. B. Coates, C. O. Weiss, C. Green, E. J. D'Angelo, and J. R. Tredicce, "Dynamical transverse laser patterns. I. Theory," *Phys. Rev. A* **49**, 1427–1451 (1994).
8. V. Yu. Bazhenov, M. S. Soskin, and M. V. Vasnetsov, "Screw dislocations in light wave fronts," *J. Mod. Opt.* **39**, 985–990 (1992).
9. N. R. Heckenberg, R. McDuff, C. P. Smith, and A. G. White, "Generation of optical phase singularities by computer-generated holograms," *Opt. Lett.* **17**, 221–223 (1992).
10. Z. S. Sacks, D. Rozas, and G. A. Swartzlander, Jr., "Holographic formation of optical vortex filaments," *J. Opt. Soc. Am. B* **15**, 2226–2234 (1998).
11. M. W. Beijersbergen, L. Allen, H. E. L. O. van der Veen, and J. P. Woerdman, "Astigmatic laser mode converters and transfer of orbital angular momentum," *Opt. Commun.* **96**, 123 (1993).
12. N. B. Baranova, B. Ya. Zel'dovich, A. V. Mamaev, N. F. Pili-petskii, and V. V. Shkunov, "Dislocations of the wavefront of a speckle-inhomogeneous field (theory and experiment)," *JETP Lett.* **33**, 195–199 (1981) [*Pis'ma Zh. Eksp. Teor. Fiz.* **33**, 206–210 (1981)].
13. G. A. Swartzlander, Jr., and C. T. Law, "Optical vortex solitons observed in Kerr nonlinear media," *Phys. Rev. Lett.* **69**, 2503–2506 (1992).
14. A. W. Snyder, L. Poladian, and D. J. Mitchell, "Stable black self-guided beams of circular symmetry in a bulk Kerr medium," *Opt. Lett.* **17**, 789–791 (1992).
15. G. A. Swartzlander, Jr., D. L. Drugan, N. Hallak, M. O. Freeman, and C. T. Law, "Optical transistor effect using an optical vortex soliton," *Laser Phys.* **5**, 704–709 (1995).
16. J. P. Gordon, R. C. C. Leite, R. S. Moore, S. P. Porto, and J.

- R. Whinnery, "Long-transient effects in lasers with inserted liquid samples," *J. Appl. Phys.* **36**, 3–7 (1965).
17. J. R. Whinnery, D. T. Miller, and F. Dabby, "Thermal convection and spherical aberration distortion of laser beams in low-loss liquids," *IEEE J. Quantum Electron.* **QE-3**, 382–383 (1968).
 18. G. A. Swartzlander, Jr., D. R. Anderson, J. J. Regan, H. Yin, and A. Kaplan, "Spatial dark-soliton stripes and grids in self-defocusing materials," *Phys. Rev. Lett.* **66**, 1583–1586 (1991).
 19. G. A. Swartzlander, Jr., B. L. Justus, A. L. Huston, A. J. Campillo, and C. T. Law, "Characteristics of a low f -number broadband visible thermal optical limiter," *Int. J. Nonlinear Opt. Phys.* **2**, 577–611 (1993).
 20. J. E. Bjorkholm and A. Ashkin, "CW self-focusing and self-trapping of light in sodium vapor," *Phys. Rev. Lett.* **32**, 129–132 (1974).
 21. G. A. Swartzlander, Jr., H. Yin, and A. E. Kaplan, "Self-bending of a cw laser beam in sodium vapor," *Opt. Lett.* **13**, 1011–1013 (1988).
 22. G. A. Swartzlander, Jr., H. Yin, and A. E. Kaplan, "Continuous-wave self-deflection effect in sodium vapor," *J. Opt. Soc. Am. B* **6**, 1317–1325 (1989).
 23. V. Tikhonenko, J. Christou, B. Luther-Davies, and Yu. S. Kivshar, "Observation of vortex solitons created by the instability of dark soliton stripes," *Opt. Lett.* **21**, 1129–1131 (1996).
 24. G. Duree, M. Morin, G. Salamo, M. Segev, B. Crosignani, P. Di Porto, E. Sharp, and A. Yariv, "Dark photorefractive spatial solitons and photorefractive vortex solitons," *Phys. Rev. Lett.* **74**, 1978 (1995).
 25. V. E. Zakharov and A. B. Shabat, "Exact theory of two-dimensional self-focusing and one-dimensional self-modulation of waves in nonlinear media," *Zh. Eksp. Teor. Fiz.* **61**, 118–134 (1971) [*Sov. Phys. JETP* **34**, 62 (1972)].
 26. V. E. Zakharov and A. B. Shabat, "Interaction between solitons in a stable medium," *Zh. Eksp. Teor. Fiz.* **64**, 1627–1639 (1973) [*Sov. Phys. JETP* **37**, 823–828 (1973)].
 27. S. A. Akhmanov, R. V. Khokhlov, and A. P. Sukhorukov, "Self-focusing, self-defocusing and self-modulation of laser beams," in *Laser Handbook*, F. T. Arecchi and E. O. Schulz-Dubois, eds. (North-Holland, Amsterdam, 1972), Vol. 2, pp. 1152–1228.
 28. M. J. Weber, ed., *CRC Handbook of Laser Science and Technology (Supplement)* (CRC Press, Boca Raton, Fla., 1991), Vol. 2.
 29. M. D. Iturbe Castillo, J. J. Sánchez-Mondragón, and S. Stepanov, "Formation of steady-state cylindrical thermal lenses in dark stripes," *Opt. Lett.* **21**, 1622–1624 (1996).
 30. M. D. Feit and J. A. Fleck, Jr., "Light propagation in gradient-index optical fibers," *Appl. Opt.* **17**, 3990–3998 (1978).